# Journal of Materials Chemistry C



View Article Online PAPER



Cite this: J. Mater. Chem. C, 2023, **11**, 3325

Received 16th December 2022. Accepted 1st February 2023

DOI: 10.1039/d2tc05374h

rsc.li/materials-c

# An effective pathway to design and synthesize UV birefringent crystals via rational assembly of $\pi$ -conjugated [CO<sub>3</sub>]<sup>2-</sup> and [NO<sub>3</sub>]<sup>-</sup> triangles†

Zhaowei Hu,<sup>a</sup> Lili Liu, o \*a Ruixin Zhang, \*b Qun Jing, \*b Huan Wang, \*a Jindan Tian, \*a Jiayue Xu\*a and P. Shiv Halasyamani 🕩 \*c

Planar  $MO_3$  (M = B, C, N) units have frequently been considered important structural components of novel birefringent crystal materials. An efficient approach for constructing new functional crystals is to simultaneously assemble multiple structural motifs together. Two compounds, Na<sub>3</sub>Rb<sub>6</sub>(CO<sub>3</sub>)<sub>3</sub>(NO<sub>3</sub>)<sub>2</sub>X· 6H<sub>2</sub>O (X = Br and Cl), were synthesized by the integration of three kinds of anionic groups. More interestingly, the  $[CO_3]^{2-}$  and  $[NO_3]^-$  groups in  $Na_3Rb_6(CO_3)_3(NO_3)_2X \cdot 6H_2O$  are all coplanar with the aid of  $[NaO_7]^{13-}$  polyhedra, which can enhance the anisotropic polarizability.  $Na_3Rb_6(CO_3)_3(NO_3)_2X\cdot 6H_2O$ have a large theoretical birefringence of  $\sim 0.165$  at 1064 nm and possess a short UV cut-off edge of  $\sim$ 230 nm. Additionally, the two compounds exhibit good crystal growth habits. These properties illustrate that Na<sub>3</sub>Rb<sub>6</sub>(CO<sub>3</sub>)<sub>3</sub>(NO<sub>3</sub>)<sub>2</sub>X·6H<sub>2</sub>O are promising UV birefringent crystals.

### Introduction

UV birefringent crystals, as a type of important functional material for optoelectronics, have important applications in optical deflection, optical modulation, and nonlinear optics. 1-5 At present, commercial UV birefringent crystals, such as CaCO<sub>3</sub>, α- $BaB_2O_4 (\alpha-BBO)^7$  and  $MgF_2$ , face some kinds of problems, such as difficulty in crystal growth, small birefringence, and an insufficient band gap, which seriously limit their practical applications. Therefore, new high-performance UV birefringent crystals are still needed.

Previous studies mainly focused on borate UV birefringent crystals, 9-12 such as SrAlB<sub>3</sub>O<sub>6</sub>F<sub>2</sub> (0.078 at 1064 nm, 7.65 eV), 13  $\text{Li}_3\text{La}_2(\text{BO}_3)_3$  (0.078 at 1064 nm, 5.22 eV), <sup>14</sup>  $\text{Ca}(\text{BO}_2)_2$  (0.247 at 193 nm, 7.34 eV), <sup>15</sup> Ba<sub>2</sub>Zn<sub>2</sub>B<sub>6</sub>O<sub>13</sub> (0.085 at 532 nm, 6.12 eV), <sup>16</sup> and NaMgBe<sub>2</sub>(BO<sub>3</sub>)<sub>2</sub>F (0.078 at 589 nm, 4.19 eV), <sup>17</sup> which is mainly attributed to the excellent properties of the planar

triangle [BO<sub>3</sub>]<sup>3-</sup> group, including the relatively strong anisotropic polarizability and high UV transmittance. 18-21 It is well known that the  $[CO_3]^{2-}$  and  $[NO_3]^{-}$  groups possess similar  $\pi$ conjugated electronic configurations and planar triangle structures to the [BO<sub>3</sub>]<sup>3-</sup> group.<sup>22,23</sup> In terms of the anisotropic polarizability of anionic groups, the trend of  $[NO_3]^- > [CO_3]^{2-}$  $> [BO_3]^{3-}$  is generally followed.<sup>24</sup> Therefore, the  $[CO_3]^{2-}$  and [NO<sub>3</sub>] groups are also ideal fundamental building blocks (FBBs) for designing birefringent materials, and they have advantages over the [BO<sub>3</sub>]<sup>3-</sup> group when building birefringent materials.<sup>25</sup>

After reviewing the inorganic crystal structure database (ICSD version 4.9.0., the last release of ICSD-2022.2), we find that there have been relatively more borate carbonates reported, but fewer nitrate borates and nitrate carbonates. Through extensive literature research, it is noticed that the pH value for synthesizing nitrate is often different from that for borate/carbonate when using solution methods. Many of the reported nitrates are synthesized under acidic conditions, for example,  $La(OH)_2NO_3$  (pH 4-6),  $^{26}$  [Pb<sub>4</sub>(OH)<sub>4</sub>](NO<sub>3</sub>)<sub>4</sub> (pH 4-5),  $^{27}$ BiGeO<sub>2</sub>(OH)<sub>2</sub>NO<sub>3</sub> (pH  $\approx$  0.2), <sup>28</sup> etc. In contrast, hexagonal H<sub>3</sub>BO<sub>3</sub> crystals will deposit from the borate system and  $[CO_3]^{2-}$  will be decomposed into CO2 molecules from the carbonate system under an acidic environment. Therefore, the coexistence of these three groups is difficult to reconcile. In recent years, several compounds have been recorded in BO<sub>3</sub>-CO<sub>3</sub> and BO<sub>3</sub>-NO<sub>3</sub> systems, such as  $Pb_7O(OH)_3(CO_3)_3(BO_3)_7^{29} Rb_9[B_4O_5(OH)_4]_3(CO_3)Br \cdot 7H_2O_7^{30} Ba_3(BO_3)$  $(CO_3)F_7^{31}K_3(B_6O_{10})(NO_3)_7^{32}Pb_6O_4(BO_3)(NO_3)_7^{33}$  and  $Pb_2(BO_3)(NO_3)_7^{34}$ while carbonate nitrates are rarely reported. In the ICSD, only ten

<sup>&</sup>lt;sup>a</sup> Institute of Crystal Growth, School of Materials Science and Engineering, Shanghai Institute of Technology, Shanghai 201418, China. E-mail: liulili@sit.edu.cn, xujiayue@sit.edu

<sup>&</sup>lt;sup>b</sup> School of Physical Science and Technology, Xinjiang University, Urumqi 830046,

<sup>&</sup>lt;sup>c</sup> Department of Chemistry, University of Houston, 112 Fleming Building, Houston, Texas 77204, USA. E-mail: psh@uh.edu

<sup>†</sup> Electronic supplementary information (ESI) available: CIF file; atomic coordinates and isotropic displacement parameters, and selected bond distances and angles; crystal structure; IR spectra; TG-DSC curves; electronic structure and PDOS. CCDC 2217264. For ESI and crystallographic data in CIF or other electronic format see DOI: https://doi.org/10.1039/d2tc05374h

Table 1 Compounds in the CO<sub>3</sub>-NO<sub>3</sub> system before 2022

Compounds	Space group	Year
$[Co(NH_3)_4(CO_3)(NO_3)]_2 \cdot H_2O^{35}$	$P2_1/n$	1990
$[Pt(NH_3)_2]_4(CO_3)_2(NO_3)_4 \cdot 3H_2O^{36}$	$P\bar{1}$	1993
$(Tl_{0.85}Cr_{0.15})Sr_4Cu_2(CO_3)_{0.5}(NO_3)_{0.5}O_7^{37}$	P4/mmm	1997
$(NH_3)_3Co(OH)_2(CO_3)Co(NH_3)_3(NO_3)_2 \cdot H_2O^{38}$	$P\bar{1}$	1999
$Co(NH_3)_5(CO_3)NO_3 \cdot H_2O^{39}$	$P2_1$	1999
(Pb <sub>6</sub> O <sub>4</sub> )(OH)(NO <sub>3</sub> )(CO <sub>3</sub> ) <sup>40</sup>	Pnma	2000
PbTiO <sub>2</sub> (CO <sub>3</sub> ) <sub>0.3</sub> (NO <sub>3</sub> ) <sub>0.35</sub> (OH) <sup>41</sup>	$P\bar{3}1m$	2001
$Ca_5(UO_2(CO_3)_3)_2(NO_3)_2 \cdot 10H_2O^{42}$	$P2_1/n$	2002
$Co(CO_3)(NH_3)_4NO_3^{43}$	$P2_1/c$	2013
(NH <sub>3</sub> ) <sub>6</sub> Rh <sub>2</sub> (CO <sub>3</sub> )(OH) <sub>2</sub> (NO <sub>3</sub> ) <sub>2</sub> ·H <sub>2</sub> O <sup>44</sup>	$P\bar{1}$	2016

compounds containing both [CO<sub>3</sub>]<sup>2-</sup> and [NO<sub>3</sub>]<sup>-</sup> groups had been reported before 2022, and their physical and chemical properties are less studied (shown in Table 1). In particular, their optical properties (such as birefringence and the SHG effect) have not been systematically studied.

Metal-centered polyhedra also have impacts on the structure and optical properties of crystals. Similar to stereochemically active lone pair (SCALP) cations or d<sup>0</sup> metal cations, they can positively affect the birefringence, 45,46 such as the SCALP Sn2+ atom in Sn<sub>2</sub>PO<sub>4</sub>I (0.664 at 532nm),<sup>47</sup> the [WO<sub>5</sub>F]<sup>5-</sup> octahedron in KWO<sub>3</sub>F (0.088 at 1064nm), 48 etc. However, these metal cations play a negative role in the transmission of UV light. 49 In the design and synthesis of UV birefringent crystals, alkali or alkaline earth metals are the preferred elements owing to the absence of electron transition of d-d and f-f orbitals, which can effectively extend the band gap. 50,51 Furthermore, compared with the O<sup>2-</sup> ion, halogen anions (F<sup>-</sup>, Cl<sup>-</sup>, and Br<sup>-</sup>) possess distinctive electronegativity, coordination ability and polarizability. So halogenated oxypolyhedra (such as the [BO<sub>3</sub>F]<sup>4-</sup>, [TiO<sub>5</sub>F]<sup>7-</sup>, and [WO<sub>5</sub>F]<sup>5-</sup> groups) always exhibit a larger polarizability than oxypolyhedra (such as the  $[BO_4]^{5-}$ ,  $[TiO_6]^{8-}$ , and [WO<sub>6</sub>]<sup>6-</sup> groups). Additionally, the addition of halogen anions usually can make the UV cutoff edge blue-shift.52

Guided by the above ideas, we successfully synthesized two mixed-alkali metal carbonate nitrate halides, Na<sub>3</sub>Rb<sub>6</sub>(CO<sub>3</sub>)<sub>3</sub>  $(NO_3)_2X\cdot 6H_2O$  (X = Br and Cl), through a hydrothermal method. During our manuscript preparation, we noticed that, quite recently, Na<sub>3</sub>Rb<sub>6</sub>(CO<sub>3</sub>)<sub>3</sub>(NO<sub>3</sub>)<sub>2</sub>Cl·6H<sub>2</sub>O was synthesized via the evaporation method by Prof. Pan's group.<sup>53</sup> Therefore, in this work, we will mainly focus on the synthesis and properties of  $Na_3Rb_6(CO_3)_3(NO_3)_2Br\cdot 6H_2O$ , but  $Na_3Rb_6(CO_3)_3(NO_3)_2Cl\cdot 6H_2O$  is also briefly described and characterized for comparison.  $Na_3Rb_6(CO_3)_3(NO_3)_2Br \cdot 6H_2O$  is the first carbonate nitrate bromide. Na<sub>3</sub>Rb<sub>6</sub>(CO<sub>3</sub>)<sub>3</sub>(NO<sub>3</sub>)<sub>2</sub>X·6H<sub>2</sub>O contains four different functional primitives, which include alkali metals (Na<sup>+</sup> and Rb<sup>+</sup>), [CO<sub>3</sub>]<sup>2-</sup>, [NO<sub>3</sub>]<sup>-</sup> and halogen anions. Their synergistic effect gives Na<sub>3</sub> Rb<sub>6</sub>(CO<sub>3</sub>)<sub>3</sub>(NO<sub>3</sub>)<sub>2</sub>X·6H<sub>2</sub>O excellent linear optical properties: large birefringence and wide UV optical band gaps. Besides, Na<sub>3</sub>Rb<sub>6</sub>(CO<sub>3</sub>)<sub>3</sub>(NO<sub>3</sub>)<sub>2</sub>X·6H<sub>2</sub>O crystals do not exhibit layered growth behavior and it is feasible to obtain their millimeter-sized crystals, ensuring the availability of large-scale single crystals. Therefore, they have the potential to serve as excellent UV birefringent crystals.

## **Experimental**

### Reagents

Ce(NO<sub>3</sub>)<sub>3</sub>·6H<sub>2</sub>O(99%), Rb<sub>2</sub>CO<sub>3</sub>(99%), NaOH(99%), NaBr(99%), and NaCl(99%) were purchased from Taitan and used as received.

### **Synthesis**

Considering that the [CO<sub>3</sub>]<sup>2-</sup> group is not stable in acidic solutions, we will try to combine the  $[CO_3]^{2-}$  and  $[NO_3]^-$  groups under neutral or alkaline conditions. Although nitrates tend to form under acidic conditions, there are still examples synthesized under alkaline condition, such as Pb<sub>2</sub>O(OH)NO<sub>3</sub> (pH = 7-8) and Pb<sub>3</sub>O<sub>2</sub>(OH)NO<sub>3</sub> (pH = 11).<sup>27</sup> After constant adjustment of raw materials and ratios, Na<sub>3</sub>Rb<sub>6</sub>(CO<sub>3</sub>)<sub>3</sub>(NO<sub>3</sub>)<sub>2</sub>X·6H<sub>2</sub>O was finally synthesized using a hydrothermal method. In the synthesis of Na<sub>3</sub>Rb<sub>6</sub>(CO<sub>3</sub>)<sub>3</sub>(NO<sub>3</sub>)<sub>2</sub>Br·6H<sub>2</sub>O, the reaction mixture of Ce(NO<sub>3</sub>)<sub>3</sub>·6H<sub>2</sub>O (1.520 g, 3.5 mmol), Rb<sub>2</sub>CO<sub>3</sub> (3.002 g, 13 mmol), NaOH (0.500 g, 12.5 mmol), NaBr (1.029 g, 10 mmol) and 5 mL of deionized water was sealed in an autoclave with a 23 mL Teflon liner. After heating at 220 °C for 2 days, the reactant was cooled to room temperature at a rate of 3  $^{\circ}$ C h<sup>-1</sup>. Similarly, single crystals of Na<sub>3</sub>Rb<sub>6</sub>(CO<sub>3</sub>)<sub>3</sub>(NO<sub>3</sub>)<sub>2</sub>Cl·6H<sub>2</sub>O were synthesized with a reaction mixture of Ce(NO<sub>3</sub>)<sub>3</sub>·6H<sub>2</sub>O (1.086 g, 2.5 mmol), Rb<sub>2</sub>CO<sub>3</sub> (3.464 g, 15 mmol), NaOH (0.800 g, 20 mmol), NaCl (0.584 g, 10 mmol) and 5 ml of deionized water. Colorless and block crystals (Fig. S1, ESI†) were obtained after washing with deionized water or ethanol. The polycrystalline powder samples of  $Na_3Rb_6(CO_3)_3(NO_3)_2Br \cdot 6H_2O$  and  $Na_3Rb_6(CO_3)_3(NO_3)_2Cl \cdot$ 6H<sub>2</sub>O were obtained directly from grinding the as-grown crystals, and their purity was checked using powder X-ray diffraction patterns (see Fig. S2, ESI†).

### Single crystal X-ray diffraction

Single crystal X-ray diffraction data of Na<sub>3</sub>Rb<sub>6</sub>(CO<sub>3</sub>)<sub>3</sub>(NO<sub>3</sub>)<sub>2</sub>Br· 6H2O and Na3Rb6(CO3)3(NO3)2Cl·6H2O were collected at room temperature by single-crystal XRD on an APEX II CCD diffractometer using monochromatic Mo-K $\alpha$  radiation ( $\lambda = 0.71073 \text{ Å}$ ). A transparent block of crystal was mounted on a glass fiber with epoxy for structure determination. Moreover, absorption corrections were carried out using the SCALE program for area detectors and integrated with the SAINT program. 54 Absorption corrections based on the multi-scan technique were also applied. The structure was resolved using the direct method and refined by full-matrix least-squares fitting on F<sup>2</sup> by SHELX-97.55 All H atoms are located at geometrically calculated positions and refined with isotropic thermal parameters. All the other atoms were refined anisotropically. All the structural data were also checked for possible missing symmetry with the program PLATON,56 and no higher symmetries were found. Relevant crystallographic data and details of the experimental conditions for  $Na_3Rb_6(CO_3)_3(NO_3)_2Br\cdot 6H_2O$  and  $Na_3Rb_6(CO_3)_3(NO_3)_2Cl\cdot 6H_2O$ are summarized in Table S1 (ESI†). Further details about atomic coordinates and isotropic displacement coefficients are supplied in Tables S2 and S3 (ESI†). Selected bond lengths are listed in

Tables S4 and S5 (ESI†). Hydrogen coordinates and isotropic displacement parameters are listed in Tables S6 and S7 (ESI†).

### Powder X-ray diffraction (PXRD)

PXRD patterns of polycrystalline materials were obtained on a TD-3500 X-ray diffractometer using Cu K $\alpha$  radiation ( $\lambda = 1.540598$  Å) at room temperature in the angular range of  $2\theta$  = 10–70° with a scan step width of 0.05° and a fixed time of 0.2 s. The PXRD patterns of the pure samples of Na<sub>3</sub>Rb<sub>6</sub>(CO<sub>3</sub>)<sub>3</sub>(NO<sub>3</sub>)<sub>2</sub>Br·6H<sub>2</sub>O and Na<sub>3</sub>Rb<sub>6</sub> (CO<sub>3</sub>)<sub>3</sub>(NO<sub>3</sub>)<sub>2</sub>Cl·6H<sub>2</sub>O show good agreement with the calculated PXRD patterns of the single-crystal models (see Fig. S2, ESI†).

### Thermal analysis

Thermogravimetric analysis (TG) and differential scanning calorimetry (DSC) were conducted on a Mettler Toledo unit. The crystal samples (5–12 mg) were enclosed in Al<sub>2</sub>O<sub>3</sub> crucibles and heated from room temperature to 800 °C at a rate of 10 °C min<sup>-1</sup> under a constant flow of nitrogen gas.

### Infrared spectroscopy

The IR spectra were recorded on a Thermo Fisher Scientific Fourier transform infrared (FT-IR) spectrometer using KBr pellets in the range of 4000-400 cm<sup>-1</sup>.

### UV-vis diffuse reflectance spectroscopy

The UV-vis diffuse reflection data were recorded at room temperature using powder samples on a Varian Cary 5000 UV/vis/NIR spectrophotometer and scanned at 200-800 nm. BaSO<sub>4</sub> was used as the standard.

### Birefringence

The birefringence  $(\Delta n)$  of Na<sub>3</sub>Rb<sub>6</sub>(CO<sub>3</sub>)<sub>3</sub>(NO<sub>3</sub>)<sub>2</sub>Br·6H<sub>2</sub>O was characterized using a polarization microscope (ZEISS Axioscope 5 pol) equipped with a Berek compensator. The average wavelength of the light source was 546 nm. The equation for calculating the birefringence is

$$R = |N_{\rm g} - N_{\rm p}| \times d = \Delta n \times d$$

Here, R represents the optical path difference;  $N_{o}$ ,  $N_{p}$  and  $\Delta n$ represent the refractive index of fast light, that of slow light, and the difference value of the refractive index, respectively; d denotes the thickness of the crystal.

### **Computational descriptions**

The first-principles calculations for the Na<sub>3</sub>Rb<sub>6</sub>(CO<sub>3</sub>)<sub>3</sub>(NO<sub>3</sub>)<sub>2</sub>  $X.6H_2O$  (X = Br and Cl) crystals were performed using the planewave pseudopotential method implemented in the CASTEP<sup>57</sup> program based on density functional theory (DFT)<sup>58</sup> with the norm-conserving pseudopotentials (NCP).<sup>59</sup> The exchange-correlation (XC) functional was described by the Perdew-Burke-Ernzerhof (PBE) functional within the generalized gradient approximation (GGA).<sup>60</sup> The crystal structure of Na<sub>3</sub>Rb<sub>6</sub>(CO<sub>3</sub>)<sub>3</sub>(NO<sub>3</sub>)<sub>2</sub>X·6H<sub>2</sub>O was optimized until the total energy, the maximum stress, the maximum atomic displacements and the maximum force were less than  $5 \times 10^{-6}$  eV per atom,  $2 \times 10^{-2}$  GPa,  $5 \times 10^{-4}$  Å, and less than  $1 \times 10^{-2}$  eV Å<sup>-1</sup>, respectively. The following valence electron configurations were used: H(1s<sup>1</sup>), C(2s<sup>2</sup>2p<sup>2</sup>), N(2s<sup>2</sup>2p<sup>3</sup>), O(2s<sup>2</sup>2p<sup>4</sup>),  $Na(2s^22p^63s^1)$ ,  $Cl(3s^23p^5)$ , and  $Rb(4s^24p^65s^1)$  for  $Na_3Rb_6(CO_3)_3$  $(NO_3)_2Cl\cdot 6H_2O$  and  $H(1s^1)$ ,  $C(2s^22p^2)$ ,  $N(2s^22p^3)$ ,  $O(2s^22p^4)$ ,  $Na(2s^22p^63s^1)$ ,  $Br(4s^24p^5)$ , and  $Rb(4s^24p^65s^1)$  for  $Na_3Rb_6(CO_3)_3$ (NO<sub>3</sub>)<sub>2</sub>Br·6H<sub>2</sub>O. The plane-wave energy cut-off for both was set at 830.0 eV. The k-point of the Monkhorst-Pack grid in the Brillouin zone for  $Na_3Rb_6(CO_3)_3(NO_3)_2X\cdot 6H_2O$  was set as  $3\times 3\times 2$  and the span of the Brillouin zone was selected as 0.04 Å<sup>-1</sup> which ensure the sufficient accuracy of the calculated results. It is well-known that the GGA method always underestimates the bandgap owing to the discontinuity of the exchange-correlation energy functional, hence a so-called scissors operator was used to calculate the optical properties.

### Results and discussion

### Structure description

Na<sub>3</sub>Rb<sub>6</sub>(CO<sub>3</sub>)<sub>3</sub>(NO<sub>3</sub>)<sub>2</sub>Br·6H<sub>2</sub>O crystallizes in the centrosymmetric space group P6<sub>3</sub>/mcm (No. 194, Table S1, ESI†). In its asymmetric unit, there is one Na atom, one Rb atom, one N atom, two C atoms, four O atoms, one Br atom and one H atom (Fig. S3 and S4, ESI†). Na<sub>3</sub>Rb<sub>6</sub>(CO<sub>3</sub>)<sub>3</sub>(NO<sub>3</sub>)<sub>2</sub>Br·6H<sub>2</sub>O exhibits a three-dimensional (3D) crystal structure consisting of  $[NaO_7]^{13-}$ ,  $[BrRb_6]^{5+}$ ,  $[CO_3]^{2-}$ ,  $[NO_3]^{-}$  and  $H_2O$  units (Fig. 1a). Each Na atom is coordinated to seven O atoms to form a  $[NaO_7]^{13-}$  polyhedron with double cones, five of which are equatorial O atoms and the rest two are apical O atoms (Fig. S5, ESI†). In [NaO<sub>7</sub>]<sup>13-</sup>, the five equatorial O atoms are connected to two edge-shared [NO<sub>3</sub>] and one corner-shared  $[C(1)O_3]^{2-}$ , and the two apical O atoms are linked to H atoms to form two  $H_2O$  groups. Then the  $[Na(CO_3)(NO_3)_2 \cdot 2H_2O]^{4-}$  polyhedron is formed, which extends infinitely in the ab plane to create the 2D  $[Na_3(CO_3)(NO_3)_2 \cdot 2H_2O]_{\infty}^-$  layer (Fig. 1b). The distance between adjacent [Na<sub>3</sub>(CO<sub>3</sub>)(NO<sub>3</sub>)<sub>2</sub>·2H<sub>2</sub>O]<sub>∞</sub> layers  $(d_{\rm Br})$  is 7.93 Å. Each Br atom is surrounded by six Rb atoms to form a [BrRb<sub>6</sub>]<sup>5+</sup> cationic octahedron (Fig. S6, ESI<sup>†</sup>). [BrRb<sub>6</sub>]<sup>5+</sup> octahedra and  $[C(2)O_3]^{2-}$  units are further connected with each other to compose the  $[(Rb_6Br)(CO_3)_2]^+_{\infty}$  layers *via* Rb-O bonds (Fig. 1c). Moreover, the  $[C(2)O_3]^{2-}$  groups are also parallel to the ab plane under the guidance of [BrRb<sub>6</sub>]<sup>5+</sup>. Eventually, [Na<sub>3</sub>(CO<sub>3</sub>)  $(NO_3)_2 \cdot 2H_2O]_{\infty}^-$  layers and  $[(Rb_6Br)(CO_3)_2]_{\infty}^+$  layers are stacked alternately along the c-axis to construct the whole structure of Na<sub>3</sub>Rb<sub>6</sub>(CO<sub>3</sub>)<sub>3</sub>(NO<sub>3</sub>)<sub>2</sub>Br·6H<sub>2</sub>O. In connectivity terms, the material may be described as a  $3[Na(CO_3)_{1/3}2(NO_3)_{1/3}\cdot 2H_2O]^{1/3}$  anion, with the charge balance maintained by the [(Rb<sub>6</sub>Br)6(CO<sub>3</sub>)<sub>1/3</sub>]<sup>+</sup> cation. Compared with Na<sub>3</sub>Rb<sub>6</sub>(CO<sub>3</sub>)<sub>3</sub>(NO<sub>3</sub>)<sub>2</sub>Br·6H<sub>2</sub>O, the layer spacing of isostructural Na<sub>3</sub>Rb<sub>6</sub>(CO<sub>3</sub>)<sub>3</sub>(NO<sub>3</sub>)<sub>2</sub>Cl·6H<sub>2</sub>O (d<sub>Cl</sub>, Fig. 1d) decreases from 7.93 Å to 7.91 Å due to the replacement of the Br ion by a smaller Cl ion.

In Na<sub>3</sub>Rb<sub>6</sub>(CO<sub>3</sub>)<sub>3</sub>(NO<sub>3</sub>)<sub>2</sub>Br·6H<sub>2</sub>O, Na-O distances are in the range of 2.303(4)-2.683(5) Å. The C-O bond distances range from 1.281(2) to 1.285(4) Å. The N-O bond distance is 1.254(4) Å. The Rb<sup>+</sup> cation is surrounded by eight O atoms and one Br atom, with Rb-O distances of 3.012(2)-3.413(3) Å and Rb-Br distance of 3.344(1) Å. All bond lengths are within

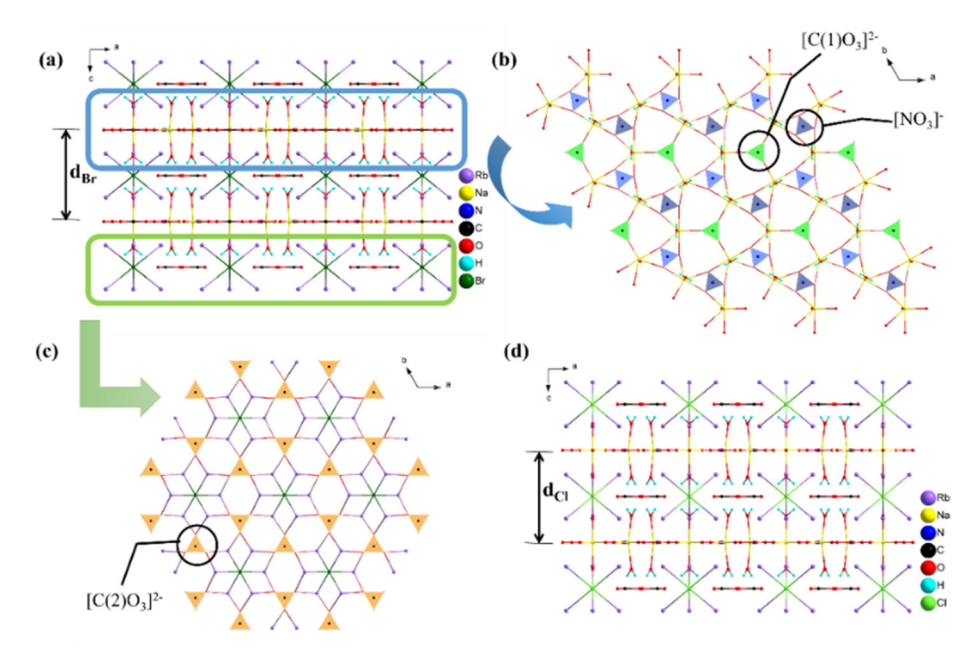


Fig. 1 (a) The crystal structure of  $Na_3Rb_6(CO_3)_3(NO_3)_2Br\cdot6H_2O$ ; (b) the  $[Na_3(CO_3)(NO_3)_2\cdot2H_2O]_0^r$  layer; and (c) the  $[(Rb_6Br)(CO_3)_2]_0^r$  layer; (d) The crystal structure of Na<sub>3</sub>Rb<sub>6</sub>(CO<sub>3</sub>)<sub>3</sub>(NO<sub>3</sub>)<sub>2</sub>Cl<sub>2</sub>6H<sub>2</sub>O. (Rb-O bonds are omitted for clarity.)

reasonable limits. The bond valence of the crystalline elements is determined using the following equation:

$$V_i = \sum_j S_{ij} = \sum_j \exp\{(r_0 - r_{ij})/B\}$$

where  $S_{ij}$  is an empirically determined parameter related to the bond lengths  $r_0$ ,  $r_{ii}$  and B (usually 0.37). <sup>61,62</sup> Bond valence sum (BVS) calculations indicate that the BVSs for Na, Rb, C(1)-C(2), N, O(1)-O(4) and Br are +1.178, +1.130, +3.992-+4.282, +4.817, -0.463--2.105, and -1.307, respectively (Table S2, ESI†). Here, O(1) has a smaller BVS value (-0.463), so it is determined to be connected with H atoms to form an H<sub>2</sub>O molecule. The elemental bond valence of Na<sub>3</sub>Rb<sub>6</sub>(CO<sub>3</sub>)<sub>3</sub>(NO<sub>3</sub>)<sub>2</sub>Cl·6H<sub>2</sub>O is listed in Table S3 (ESI<sup>†</sup>).

### Structure-property relationship

 $\pi$ -conjugated MO<sub>3</sub> (M = B, N and C) groups are ideal functional motifs for birefringent materials because of their large anisotropic polarizability. The appropriate arrangement of MO<sub>3</sub> groups has a strong influence on the macroscopic optical properties of crystals. For example, compounds NaZnCO<sub>3</sub>F and Na<sub>4</sub>Zn(CO<sub>3</sub>)<sub>3</sub>, reported by Ye's group, have the same functional unit the  $\pi$ -conjugated  $[CO_3]^{2-}$  group. In terms of their crystal structures, the [CO<sub>3</sub>]<sup>2-</sup> groups in NaZnCO<sub>3</sub>F are arranged in a coplanar manner, but the [CO<sub>3</sub>]<sup>2-</sup> groups in Na<sub>4</sub>Zn(CO<sub>3</sub>)<sub>3</sub> point in different directions.<sup>63</sup> The different arrangements of the [CO<sub>3</sub>]<sup>2-</sup> groups make NaZnCO<sub>3</sub>F have a larger birefringence of 0.171 at 1064 nm, and Na<sub>4</sub>Zn(CO<sub>3</sub>)<sub>3</sub> have a relatively smaller birefringence of 0.138 at 1064 nm.

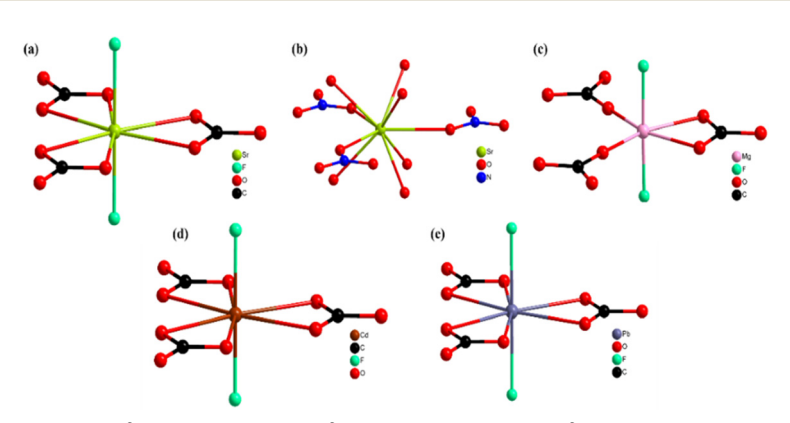


Fig. 2 The coordination environments of  $Sr^{2+}$  in  $RbSrCO_3F$  (a),  $Sr^{2+}$  in  $Sr_2(OH)_3NO_3$  (b),  $Mg^{2+}$  in  $RbMgCO_3F$  (c),  $Cd^{2+}$  in  $KCdCO_3F$  (d) and  $Pb^{2+}$  in CsPbCO<sub>3</sub>F (e).

Therefore, the coplanar arrangement is the optimum choice, which can promote effective superposition of microcosmic anisotropic polarizability.

Then, how to achieve the coplanar arrangement of the MO<sub>3</sub> group? From the well-known ABCO<sub>3</sub>F system, it can be realized that the equatorial O atoms can efficiently direct MO<sub>3</sub> for the coplanar arrangement. Moreover, we found that the oxypolyhedra formed by divalent metal cations can provide equatorial O atoms, such as Sr2+ in RbSrCO3F64 (Fig. 2a) and Sr2(OH)3NO3 (Fig. 2b),<sup>65</sup> Mg<sup>2+</sup> in RbMgCO<sub>3</sub>F (Fig. 2c),<sup>66</sup> Cd<sup>2+</sup> in KCdCO<sub>3</sub>F (Fig. 2d),<sup>67</sup> and Pb<sup>2+</sup> in CsPbCO<sub>3</sub>F (Fig. 2e).<sup>68</sup> But it is rarely reported that alkali metal-centered oxypolyhedra offer equatorial O atoms. Interestingly, the [NaO<sub>7</sub>]<sup>13-</sup> polyhedron in Na<sub>3</sub>Rb<sub>6</sub>(CO<sub>3</sub>)<sub>3</sub>(NO<sub>3</sub>)<sub>2</sub>Br-6H<sub>2</sub>O (this work) has five equatorial O atoms, and the same situation happened in Na<sub>3</sub>Rb<sub>6</sub>(CO<sub>3</sub>)<sub>3</sub>(NO<sub>3</sub>)<sub>2</sub>Cl·6H<sub>2</sub>O, which prompts

us to study related systems (Fig. 1a). We investigated two systems including mixed-alkali metal carbonates and mixed-alkali metal nitrates to study the phenomenon of alkali metal cations supplying equatorial O atoms. There are eleven compounds in the two systems according to the ICSD (listed in Table 2), and only five of them possess equatorial O atoms: NaRb<sub>2</sub>(NO<sub>3</sub>)<sub>3</sub>,<sup>69</sup> NaA<sub>2</sub>(HCO<sub>3</sub>)(CO<sub>3</sub>)·  $2H_2O (A = K \text{ and } Rb)$ , <sup>70</sup>  $Na_3Rb_6(CO_3)_3(NO_3)_2Cl\cdot 6H_2O$ , <sup>53</sup> and  $Na_3Rb_6$ (CO<sub>3</sub>)<sub>3</sub>(NO<sub>3</sub>)<sub>2</sub>Br·6H<sub>2</sub>O (this work). In NaRb<sub>2</sub>(NO<sub>3</sub>)<sub>3</sub>, Na<sup>+</sup> is connected with eight O atoms, six of which are equatorial O atoms from three bidentate [NO<sub>3</sub>]<sup>-</sup>. While in NaA<sub>2</sub>(HCO<sub>3</sub>)(CO<sub>3</sub>)·2H<sub>2</sub>O, Na<sup>+</sup> is bonded to six O atoms, and only four of them are equatorial O atoms linking with two bidentate [CO<sub>3</sub>]<sup>2-</sup>. However, Na<sup>+</sup> in Na<sub>3</sub>Rb<sub>6</sub>(CO<sub>3</sub>)<sub>3</sub> (NO<sub>3</sub>)<sub>2</sub>X·6H<sub>2</sub>O has five equatorial O atoms, four of which are from two bidentate [NO<sub>3</sub>] groups and the rest one is from a monodentate [CO<sub>3</sub>]<sup>2-</sup> group. Through literature research and structural

Table 2 Mixed-alkali metal carbonates and mixed-alkali metal nitrates. (A' = alkali metals with smaller atomic numbers; A'' = alkali metals with larger atomic numbers)

Molecular formula	$\mathbf{A}'$	$A^{\prime\prime}$	$A^{\prime\prime}/A^\prime$	$A'O_n$ unit	$A''O_n$ unit	Equatorial O atoms
KRb <sub>2</sub> CO <sub>3</sub> F <sup>71</sup>	K	Rb	Disordered structure			
LiNaCO <sub>3</sub> <sup>72</sup>	Li	Na	1.562		7	None
${\rm LikCO_3}^{73}$	Li	K	2.192	1	*	None
LiRbCO <sub>3</sub> <sup>73</sup>	Li	Rb	2.329	7	*	None
LiCsCO <sub>3</sub> <sup>73</sup>	Li	Cs	2.671	7	*	None
$\rm NaKCO_3 \cdot 6H_2O^{74}$	Na	K	1.310		*	None
$NaK_2(HCO_3)(CO_3) \cdot 2H_2O^{70}$	Na	K	1.422	-	*	Four
$NaRb_2(HCO_3)(CO_3)\cdot 2H_2O^{70}$	Na	Rb	1.509	-	*	Four
$Na_3Rb_6(CO_3)_3(NO_3)_2Cl\cdot 6H_2O^{53}$	Na	Rb	1.452	-	*	Five
$Na_3Rb_6(CO_3)_3(NO_3)_2Br\cdot 6H_2O^a$	Na	Rb	1.452	-	*	Five
$NaRb_2(NO_3)_3^{69}$	Na	Rb	1.386	*	X	Six

<sup>&</sup>lt;sup>a</sup> The compound synthesized in this work.

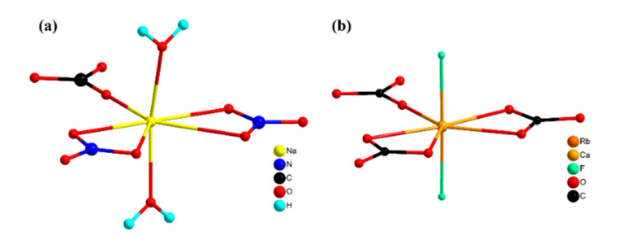


Fig. 3 The coordination environments of (a) Na<sup>+</sup> in Na<sub>3</sub>Rb<sub>6</sub>(CO<sub>3</sub>)<sub>3</sub>(NO<sub>3</sub>)<sub>2</sub> Br·6H<sub>2</sub>O and (b) Ca<sup>2+</sup> in RbCaCO<sub>3</sub>F.

comparison, it was found that Na<sup>+</sup> in Na<sub>3</sub>Rb<sub>6</sub>(CO<sub>3</sub>)<sub>3</sub>(NO<sub>3</sub>)<sub>2</sub>X·6H<sub>2</sub>O (this work) is similar to Ca2+ in RbCaCO3F64 from the ABCO3F family, and both of them are seven coordinated and have five equatorial O atoms to direct the MO<sub>3</sub> groups to be coplanar (Fig. 3).

An appropriate ionic radius has an essential effect on the formation of equatorial O atoms. In Table 2, it is noticed that the cation with a too large or small radius does not have equatorial atoms. For example, Li<sup>+</sup> ions in LiACO<sub>3</sub> (A = Na, K, Rb, Cs) are four or five-coordinated, and these  $[LiO_4]^{7-}$  or [LiO<sub>5</sub>]<sup>9-</sup> groups do not have equatorial atoms, which is probably because the Li atom is too small to bond with enough O atoms to form the equatorial plane. If the cation radius is too large, it will impede the formation of the equatorial plane, because large cations usually may attract too many O atoms as ligands and make the O atoms deviate from the equatorial plane, like the A" atoms in Table 2. Therefore, the cations with moderate radius can promote the construction of the equatorial O plane and then guide the arrangement of planar MO3 groups. It is found that all the equatorial O atoms appear in the Na-centered polyhedra in Table 2, which demonstrates that Na<sup>+</sup> possesses a suitable ionic radius. Inspired by Zou's work, 64 we speculated that the number of equatorial O atoms is related to the radius ratio of different cations. So, we calculated the cation radius ratio (A"/A' ratio) of the compounds listed in Table 2. It illustrates that when the A"/A' ratio is between 1.386 and 1.509, equatorial O atoms will appear, otherwise, they will not exist. In addition, the number of equatorial O decreases with the increase of the A"/A' ratio. Therefore, the choice of cation is crucial in the design and synthesis of planar group optical materials, which has a significant effect on the structure and properties of materials.

#### Thermal behaviour

The TG-DSC curves of Na<sub>3</sub>Rb<sub>6</sub>(CO<sub>3</sub>)<sub>3</sub>(NO<sub>3</sub>)<sub>2</sub>Br·6H<sub>2</sub>O are shown in Fig. S7a (ESI†). It is stable until  $\sim 100$  °C, and the significant weight loss is presumably attributed to the absence of crystal water. The graph shows a weight loss ratio of 9.76%, which is basically consistent with the theoretical calculation of 10.06%. The decomposition of Na<sub>3</sub>Rb<sub>6</sub>(CO<sub>3</sub>)<sub>3</sub>(NO<sub>3</sub>)<sub>2</sub>Br·6H<sub>2</sub>O has also occurred at the same time. The remaining chemicals are mainly RbBr, RbNO<sub>3</sub> and Na<sub>2</sub>CO<sub>3</sub> (Fig. S8a, ESI†). The peak around 350 °C represents the melting point. The weightlessness after 600 °C is due to the volatilization of residues. Na<sub>3</sub>Rb<sub>6</sub>(CO<sub>3</sub>)<sub>3</sub>(NO<sub>3</sub>)<sub>2</sub>Cl·6H<sub>2</sub>O exhibits similar trends (Fig. S7b, ESI†).

### IR and UV-vis diffuse reflectance spectra

The IR spectrum of Na<sub>3</sub>Rb<sub>6</sub>(CO<sub>3</sub>)<sub>3</sub>(NO<sub>3</sub>)<sub>2</sub>Br·6H<sub>2</sub>O is shown in Fig. S9a (ESI†). The stretching of O-H leads to large broad bands at 3104 cm<sup>-1</sup> and around 2423 cm<sup>-1</sup>. The stretching vibrations of C-O and N-O can be reflected by the peaks around 1400 cm<sup>-1</sup>. The out-of-plane and bending vibrations of C-O-C can be observed at 864 cm<sup>-1</sup> and 702 cm<sup>-1</sup>, and the peaks at 825 cm<sup>-1</sup> and 794 cm<sup>-1</sup> reflect the nonplanar bending vibration of the [NO<sub>3</sub>]<sup>-</sup> triangular group. Na<sub>3</sub>Rb<sub>6</sub>(CO<sub>3</sub>)<sub>3</sub>(NO<sub>3</sub>)<sub>2</sub>Cl· 6H<sub>2</sub>O also possesses similar peaks (Fig. S9b, ESI†).

The UV-vis diffuse reflectance spectra of Na<sub>3</sub>Rb<sub>6</sub>(CO<sub>3</sub>)<sub>3</sub>(NO<sub>3</sub>)<sub>2</sub> X-6H<sub>2</sub>O were recorded using the powder samples. As shown in Fig. 4, the reflectance for Na<sub>3</sub>Rb<sub>6</sub>(CO<sub>3</sub>)<sub>3</sub>(NO<sub>3</sub>)<sub>2</sub>Br·6H<sub>2</sub>O at 230 nm is about 13%, and the value for Na<sub>3</sub>Rb<sub>6</sub>(CO<sub>3</sub>)<sub>3</sub>(NO<sub>3</sub>)<sub>2</sub>Cl·6H<sub>2</sub>O at 228 nm is about 5%, which illustrates that the UV cut-off edges of  $Na_3Rb_6(CO_3)_3(NO_3)_2Br\cdot 6H_2O$  and  $Na_3Rb_6(CO_3)_3(NO_3)_2Cl\cdot 6H_2O$  are shorter than 230 nm and 228 nm, respectively, and the corresponding energy band gaps are 4.80 eV and 4.90 eV respectively. The above data indicate that Na<sub>3</sub>Rb<sub>6</sub>(CO<sub>3</sub>)<sub>3</sub>(NO<sub>3</sub>)<sub>2</sub>X·6H<sub>2</sub>O are potentially capable of UV region applications and may have a relatively large laser damage threshold.

### Theoretical calculations

To further understand the relationship between the electronic structure and optical properties of Na<sub>3</sub>Rb<sub>6</sub>(CO<sub>3</sub>)<sub>3</sub>(NO<sub>3</sub>)<sub>2</sub>X·6H<sub>2</sub>O, theoretical calculations were performed based on DFT. The calculated band structure (Fig. S10, ESI†) shows that Na<sub>3</sub>Rb<sub>6</sub> (CO<sub>3</sub>)<sub>3</sub>(NO<sub>3</sub>)<sub>2</sub>Br·6H<sub>2</sub>O and Na<sub>3</sub>Rb<sub>6</sub>(CO<sub>3</sub>)<sub>3</sub>(NO<sub>3</sub>)<sub>2</sub>Cl·6H<sub>2</sub>O are direct band-gap compounds with the valence band maximum (VBM) and

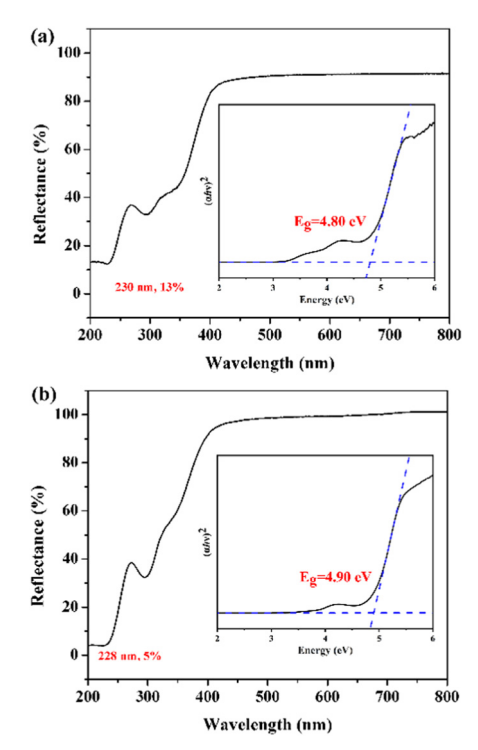
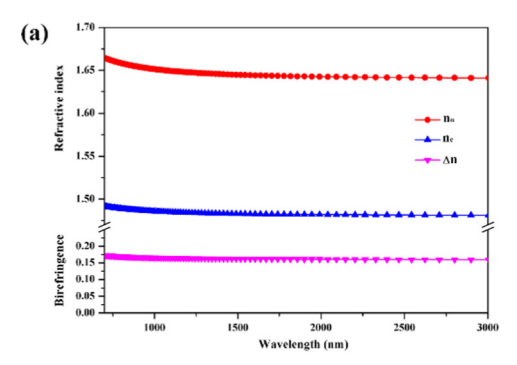


Fig. 4 UV-vis diffuse reflectance spectra of (a) Na<sub>3</sub>Rb<sub>6</sub>(CO<sub>3</sub>)<sub>3</sub>(NO<sub>3</sub>)<sub>2</sub>Br-6H<sub>2</sub>O and (b) Na<sub>3</sub>Rb<sub>6</sub>(CO<sub>3</sub>)<sub>3</sub>(NO<sub>3</sub>)<sub>2</sub>Cl·6H<sub>2</sub>O.



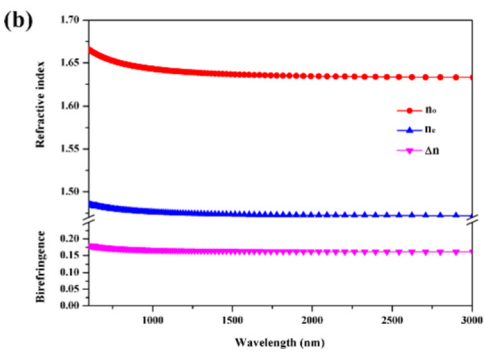


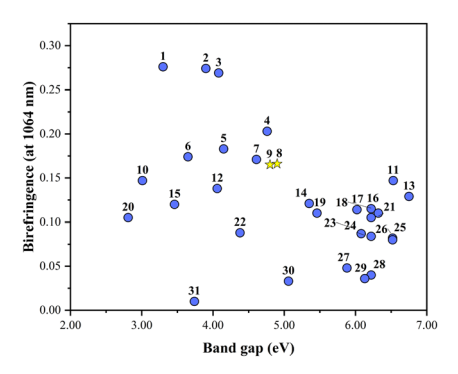
Fig. 5 The calculated refractive index and birefringence curves of (a)  $Na_3Rb_6(CO_3)_3(NO_3)_2Br\cdot 6H_2O$  and (b)  $Na_3Rb_6(CO_3)_3(NO_3)_2Cl\cdot 6H_2O$ 

the conduction band minimum (CBM) at the G point. The GGA-PBE band gaps of Na<sub>3</sub>Rb<sub>6</sub>(CO<sub>3</sub>)<sub>3</sub>(NO<sub>3</sub>)<sub>2</sub>Br·6H<sub>2</sub>O and Na<sub>3</sub>Rb<sub>6</sub> (CO<sub>3</sub>)<sub>3</sub>(NO<sub>3</sub>)<sub>2</sub>Cl·6H<sub>2</sub>O are calculated to be 1.77 eV and 1.85 eV, respectively, which are smaller than the measured values because of the discontinuity of the exchange-correlation functional.

To understand the composition and origination of the electronic structures, the total density of states (TDOS) and projected density of states (PDOS) are obtained (Fig. S10, ESI†). As shown in Fig. S10 (ESI†), for Na<sub>3</sub>Rb<sub>6</sub>(CO<sub>3</sub>)<sub>3</sub>(NO<sub>3</sub>)<sub>2</sub>Br·6H<sub>2</sub>O, O-2p, C-2p, Rb-4p, Rb-4s and Br-3p states mainly occupy the gap from -6 to -1 eV. The VBM of Na<sub>3</sub>Rb<sub>6</sub>(CO<sub>3</sub>)<sub>3</sub>(NO<sub>3</sub>)<sub>2</sub>Br·6H<sub>2</sub>O is mainly composed of O-2p, N-2p, Rb-4s, Rb-4p, Na-2p, and a small amount of Br-s orbitals; the CBM of Na<sub>3</sub>Rb<sub>6</sub>(CO<sub>3</sub>)<sub>3</sub>(NO<sub>3</sub>)<sub>2</sub>Br·6H<sub>2</sub>O is mainly composed of Rb-s as well as Br-s orbitals. For Na<sub>3</sub>Rb<sub>6</sub>(CO<sub>3</sub>)<sub>3</sub>(NO<sub>3</sub>)<sub>2</sub>Cl·6H<sub>2</sub>O (Fig. S10, ESI†), it is mainly occupied by the O-2p, C-2p, Rb-4p, Rb-4s and Cl-3p states from -6 to -1 eV. The VBM of Na<sub>3</sub>Rb<sub>6</sub>(CO<sub>3</sub>)<sub>3</sub>(NO<sub>3</sub>)<sub>2</sub>Cl·6H<sub>2</sub>O is dominated by O-2p and H-1s states. The CBM of Na<sub>3</sub>Rb<sub>6</sub>(CO<sub>3</sub>)<sub>3</sub> (NO<sub>3</sub>)<sub>2</sub>Cl·6H<sub>2</sub>O is mainly dominated by N-2p, O-2p and a little part from Na-2p, Rb-4p, and Rb-4s orbitals. It is well known that the electronic transition from the VBM to the CBM near the Fermi level determines the optical performance of optical materials. Thus, the linear optical properties of Na<sub>3</sub>Rb<sub>6</sub>(CO<sub>3</sub>)<sub>3</sub>(NO<sub>3</sub>)<sub>2</sub>X·6H<sub>2</sub>O are mainly determined by the  $\pi$ -conjugated  $[CO_3]^{2-}$  and  $[NO_3]^-$  groups.

### Linear optical properties

The linear optical properties can be obtained using the dielectric function  $\varepsilon(\omega) = \varepsilon_1(\omega) + i\varepsilon_2(\omega)$ . The obtained curve of birefringence versus wavelength is shown in Fig. 5. The calculated refractive indices and birefringence curves reveal that Na<sub>3</sub>Rb<sub>6</sub>(CO<sub>3</sub>)<sub>3</sub>(NO<sub>3</sub>)<sub>2</sub>X·6H<sub>2</sub>O are negative uniaxial crystals. Their



No.	Molecular formula	No.	Molecular formula
1	$Pb_6O_4(BO_3)(NO_3)$	17	NaZnCO₃(OH)
2	KPb <sub>2</sub> (CO <sub>3</sub> ) <sub>2</sub> F	18	LiKCO <sub>3</sub>
3	$In(IO_3)_2(NO_3)$	19	KCdCO₃F
4	La(OH)₂NO₃	20	$Cs_3VO(O_2)_2CO_3$
5	CsPbCO₃F	21	KY(CO <sub>3</sub> ) <sub>2</sub>
6	$Pb_2(BO_3)(NO_3)$	22	$Lu_8O(CO_3)_3(OH)_{15}Br$
7	NaZnCO₃F	23	Zn(NH <sub>3</sub> )CO <sub>3</sub>
8	$Na_3Rb_6(CO_3)_3(NO_3)_2CI\cdot 6H_2O$	24	$Na_2Gd(CO_3)F_3$
9	$Na_3Rb_6(CO_3)_3(NO_3)_2Br\cdot 6H_2O$	25	$Ca_2Na_3(CO_3)_3F$
10	$Cs_2Pb(NO_3)_2Br_2$	26	$Ba_2NO_3(OH)_3$
11	LiZn(OH)CO₃	27	$Ba_3(BO_3)(CO_3)F$
12	$Na_4Zn(CO_3)_3$	28	$(NH_4)_2Ca_2Y_4(CO_3)_9\cdot H_2O$
13	RbMgCO₃F	29	$Cs_3B_8O_{13}(NO_3)$
14	RbCdCO₃F	30	$Ba_2B_5O_8(OH)_2(NO_3)\cdot 3H_2O$
15	$Sr_3[SnOSe_3][CO_3]$	31	$Na_{10}Cd(NO_3)_4(SO_3S)_4$
16	RbCaCO₃F		

Fig. 6 Birefringence and band gap statistics of selected carbonates and nitrates.

birefringence values are 0.165 and 0.166 at 1064 nm for  $Na_3Rb_6(CO_3)_3(NO_3)_2Br\cdot 6H_2O$  and  $Na_3Rb_6(CO_3)_3(NO_3)_2Cl\cdot 6H_2O$ , respectively.

A real-space atom-cutting (RSAC) method has been used to intuitively exhibit the contribution of the  $[CO_3]^{2-}$  and  $[NO_3]^{-}$ groups. Following the rule of keeping the cutting spheres in contact and avoiding overlap, the cutting radii are set to be 1.48 Å (Rb), 1.25 Å (Na), 1.60 Å(C), 1.23 Å (N), 0.35 Å (H), 1.10 Å (O), 1.55 Å (Br) and 1.50 Å (Cl). Table S8 (ESI†) shows that the main contribution to the birefringence is derived from the [CO<sub>3</sub>]<sup>2-</sup> and [NO<sub>3</sub>] groups. From the birefringence of the decomposed groups,  $[NO_3]^-$  exhibits a birefringence ( $\sim 0.121$  at 1064 nm) larger than that of  $[CO_3]^{2-}$  ( $\sim 0.090$  at 1064 nm).

The birefringence of Na<sub>3</sub>Rb<sub>6</sub>(CO<sub>3</sub>)<sub>3</sub>(NO<sub>3</sub>)<sub>2</sub>Br·6H<sub>2</sub>O was preliminarily evaluated using a polarized light microscope (Fig. S11, ESI†). The measured direction was chosen randomly and the average thickness of the selected crystal is  $\sim$  7 µm with an optical path difference of 855 nm at 546 nm. So, the corresponding birefringence of Na<sub>3</sub>Rb<sub>6</sub>(CO<sub>3</sub>)<sub>3</sub>(NO<sub>3</sub>)<sub>2</sub>Br·6H<sub>2</sub>O along the measured direction is  $\sim 0.12$ , close to the value of  $Na_3Rb_6(CO_3)_3(NO_3)_2Cl\cdot 6H_2O$  reported in ref. 53.

Birefringence and band gap are important criteria for UV birefringent crystals; however, they are essentially opponents. Fig. 6 shows the birefringence values and band gaps of some carbonates and nitrates (see Table S9 ESI† for detailed values), and it can be seen that both Na<sub>3</sub>Rb<sub>6</sub>(CO<sub>3</sub>)<sub>3</sub>(NO<sub>3</sub>)<sub>2</sub>X·6H<sub>2</sub>O have relatively well balanced linear optical properties.

### Conclusions

In summary, we succeeded in enabling the  $[CO_3]^{2-}$  and  $[NO_3]^{-}$ groups to co-exist in one structure and obtained two isostructural compounds Na<sub>3</sub>Rb<sub>6</sub>(CO<sub>3</sub>)<sub>3</sub>(NO<sub>3</sub>)<sub>2</sub>Br·6H<sub>2</sub>O and Na<sub>3</sub>Rb<sub>6</sub> (CO<sub>3</sub>)<sub>3</sub>(NO<sub>3</sub>)<sub>2</sub>Cl·6H<sub>2</sub>O. Although both compounds were characterized in this work, the synthesis and properties of Na<sub>3</sub>Rb<sub>6</sub>(CO<sub>3</sub>)<sub>3</sub>(NO<sub>3</sub>)<sub>2</sub>Br·6H<sub>2</sub>O were paid more attention. In the structure of Na<sub>3</sub>Rb<sub>6</sub>(CO<sub>3</sub>)<sub>3</sub>(NO<sub>3</sub>)<sub>2</sub>Br·6H<sub>2</sub>O, the five equatorial O atoms of [NaO<sub>7</sub>]<sup>13-</sup> groups help the [CO<sub>3</sub>]<sup>2-</sup> and [NO<sub>3</sub>]<sup>-</sup> groups arrange in a coplanar manner, resulting in the most favorable superposition of anisotropic polarization. Benefiting from the optimized crystal structure, Na<sub>3</sub>Rb<sub>6</sub>(CO<sub>3</sub>)<sub>3</sub>(NO<sub>3</sub>)<sub>2</sub>Br·6H<sub>2</sub>O has a large birefringence of 0.165 at 1064 nm based on theoretical calculations. Moreover, the experimental birefringence is about 0.12 at 546 nm. In addition, its UV cut-off edges can reach 230 nm. The desired balance between the birefringence and band gap proves that Na<sub>3</sub>Rb<sub>6</sub>(CO<sub>3</sub>)<sub>3</sub>(NO<sub>3</sub>)<sub>2</sub>Br·6H<sub>2</sub>O could be a promising UV birefringent crystal. Furthermore, it is noticed that a moderate ionic radius and a suitable radius ratio of cations are essential for the formation of equatorial O atoms, so the selection of an appropriate cation plays a pivotal role in the design and synthesis of optical materials based on planar groups. The successful syntheses of carbonate nitrates give more possibilities for exploring new compounds, and we also expect that our study on the structure-property relationship will contribute to the discovery of more novel functional crystal materials.

### Conflicts of interest

There are no conflicts to declare.

## Acknowledgements

The authors acknowledge the financial support from the Shanghai Pujiang Program (20PJ1412900), Scientific Research Foundation of Shanghai Institute of Technology (YJ2021-5), the Welch Foundation (Grant E-1457) and the NSF (DMR-2002319).

### Notes and references

- 1 C. Lin, A. Zhou, W. Cheng, N. Ye and G. Chai, *J. Phys. Chem. C*, 2019, **123**, 31183–31189.
- S. Niu, G. Joe, H. Zhao, Y. Zhou, T. Orvis, H. Huyan, J. Salman,
  K. Mahalingam, B. Urwin, J. Wu, Y. Liu, T. E. Tiwald,
  S. B. Cronin, B. M. Howe, M. Mecklenburg, R. Haiges,
  D. J. Singh, H. Wang, M. A. Kats and J. Ravichandran, *Nat. Photonics*, 2018, 12, 392–396.
- 3 H. Yang, H. Jussila, A. Autere, H. Komsa, G. Ye, X. Chen, T. Hasan and Z. Sun, *ACS Photonics*, 2017, 4, 3023–3030.
- 4 H. Liu, H. Wu, H. Yu, Z. Hu, J. Wang and Y. Wu, *J. Mater. Chem. C*, 2021, **9**, 15321–15328.
- 5 L. Liu, B. Zhang, P. S. Halasyamani and W. Zhang, J. Mater. Chem. C, 2021, 9, 6491–6497.
- 6 G. Ghosh, Opt. Commun., 1999, 163, 95-102.

- 7 G. Zhou, J. Xu, X. Chen, H. Zhong, S. Wang, K. Xu, P. Deng and F. Gan, J. Cryst. Growth, 1998, 191, 517–519.
- 8 F. Sedlmeir, R. Zeltner, G. Leuchs and H. G. Schwefel, *Opt. Express*, 2014, **22**, 30934–30942.
- 9 C. Huang, M. Mutailipu, F. Zhang, K. J. Griffith, C. Hu, Z. Yang, J. M. Griffin, K. R. Poeppelmeier and S. Pan, *Nat. Commun.*, 2021, 12, 2597.
- 10 X. Li and G. Yang, Inorg. Chem., 2022, 61, 10205-10210.
- 11 S. Han, Y. Wang, B. Zhang, Z. Yang and S. Pan, *Inorg. Chem.*, 2018, 57, 873–878.
- 12 C. Huang, G. Han, H. Li, F. Zhang, Z. Yang and S. Pan, Dalton Trans., 2019, 48, 6714–6717.
- 13 S. Bai, X. Zhang, B. Zhang, L. Li and Y. Wang, *Inorg. Chem.*, 2021, **60**, 10006–10011.
- 14 X. Shi, W. Zhang, W. Cai, S. Han, Z. Yang and S. Pan, *Inorg. Chem.*, 2021, 60, 12565–12572.
- 15 X. Chen, B. Zhang, F. Zhang, Y. Wang, M. Zhang, Z. Yang, K. R. Poeppelmeier and S. Pan, *J. Am. Chem. Soc.*, 2018, **140**, 16311–16319.
- 16 R. Zhang, X. Su, J. Zhang, D. Wen and Y. Huang, Chem. Commun., 2022, 58, 10182–10185.
- 17 R. Guo, X. Jiang, S. Guo, M. Xia, L. Liu, Z. Lin and X. Wang, Inorg. Chem., 2022, 61, 7624–7630.
- 18 C. Jin, F. Li, B. Cheng, H. Qiu, Z. Yang, S. Pan and M. Mutailipu, Angew. Chem., Int. Ed., 2022, 61, e202203984.
- 19 Y. Li, X. Chen and K. M. Ok, *Chem. Commun.*, 2022, 58, 8770–8773.
- 20 S. Li, X. Liu, H. Wu, Z. Song, H. Yu, Z. Lin, Z. Hu, J. Wang and Y. Wu, *Chem. Sci.*, 2021, **12**, 13897–13901.
- 21 W. Zhang, J. Huang, S. Han, Z. Yang and S. Pan, *J. Am. Chem. Soc.*, 2022, **144**, 9083–9090.
- 22 L. Cao, Y. Song, G. Peng, M. Luo, Y. Yang, C. Lin, D. Zhao, F. Xu, Z. Lin and N. Ye, *Chem. Mater.*, 2019, 31, 2130–2137.
- 23 Y. Long, X. Dong, H. Zeng, Z. Lin and G. Zou, *Inorg. Chem.*, 2022, 61, 4184–4192.
- 24 R. Li, Z. Kristallogr., 2013, 228, 526-531.
- 25 X. Dong, L. Huang, Q. Liu, H. Zeng, Z. Lin, D. Xu and G. Zou, *Chem. Commun.*, 2018, 54, 5792–5795.
- 26 Y. Song, M. Luo, C. Lin and N. Ye, Chem. Mater., 2017, 29, 896–903.
- 27 G. Wang, M. Luo, N. Ye, C. Lin and W. Cheng, *Inorg. Chem.*, 2014, **53**, 5222–5228.
- 28 K. Kobayashi, T. Ikeda, N. Hiyoshi and Y. Sakka, *CrystEng-Comm*, 2014, **16**, 10080–10088.
- 29 M. Abudoureheman, L. Wang, X. Zhang, H. Yu, Z. Yang, C. Lei, J. Han and S. Pan, *Inorg. Chem.*, 2015, 54, 4138–4142.
- 30 L. Liu, Y. Yang, J. Huang, X. Dong, Z. Yang and S. Pan, *Chem. Eur. J.*, 2017, 23, 10451-10459.
- 31 C. Huang, F. Zhang, S. Cheng, Z. Yang, H. Li and S. Pan, *Chem. Eur. J.*, 2020, **26**, 16628–16632.
- 32 Q. Zhang, F. Zhang, F. Li, S. Han, Z. Yang and S. Pan, *Eur. J. Inorg. Chem.*, 2021, 1297–1304.
- 33 S. Bai, D. Yang, B. Zhang, L. Li and Y. Wang, *Dalton Trans.*, 2022, **51**, 3421–3425.
- 34 J. Song, C. Hu, X. Xu, F. Kong and J. Mao, *Angew. Chem., Int. Ed.*, 2015, **127**, 3750–3753.

Paper

- 35 I. Bernal and J. Cetrullo, Struct. Chem., 1990, 1, 227-234.
- 36 H. K. Mahtani, S. Chang, J. R. Ruble, I. N. L. Black and P. B. Stein, Inorg. Chem., 1993, 32, 4976-4978.
- 37 A. Barnabé, F. Letouzé, D. Pelloquin, A. Maignan, M. Hervieu and B. Raveau, Chem. Mater., 1997, 9, 2205-2211.
- 38 A. Norlund Christencen and R. G. Hazell, Acta Chem. Scand., 1999, 53, 399-402.
- 39 J. Zhu, H. Wu and A. Le Bail, Solid State Sci., 1999, 1, 55-62.
- 40 Y. Li, S. V. Krivovichev and P. C. Burns, J. Solid State Chem., 2000, 153, 365-370.
- 41 G. R. Blake, A. R. Armstrong, E. Sastre, W. Zhoua and P. A. Wright, Mater. Res. Bull., 2001, 36, 1837-1845.
- 42 Y. Li and P. C. Burns, J. Solid State Chem., 2002, 166,
- 43 A. Le Bail, Acta Crystallogr., Sect. E: Struct. Rep. Online, 2013, E69, i42-i43.
- 44 S. N. Vorob'eva, I. A. Baidina and I. V. Korol'kov, J. Struct. Chem., 2016, 57, 1588-1592.
- 45 J. Jiao, F. Liang, C. Li, T. Han, W. Zhao, Y. She, N. Ye, Z. Hu and Y. Wu, Inorg. Chem., 2022, 61, 11471-11477.
- 46 Y. Deng, L. Huang, X. Dong, L. Wang, K. M. Ok, H. Zeng, Z. Lin and G. Zou, Angew. Chem., Int. Ed., 2020, 59, 21151-21156.
- 47 J. Guo, A. Tudi, S. Han, Z. Yang and S. Pan, Angew. Chem., Int. Ed., 2021, 60, 24901-24904.
- 48 H. Tang, R. Fu, Z. Ma and X. Wu, Inorg. Chem., 2021, 60, 17364-17370.
- 49 H. Yu, W. Zhang, J. Young, J. M. Rondinelli and P. S. Halasyamani, J. Am. Chem. Soc., 2016, 138, 88-91.
- 50 J. Jiao, M. Cheng, R. Yang, Y. Yan, M. Zhang, F. Zhang, Z. Yang and S. Pan, Angew. Chem., Int. Ed., 2022, 61, e202205060.
- 51 G. Shi, F. Zhang, B. Zhang, D. Hou, X. Chen, Z. Yang and S. Pan, Inorg. Chem., 2017, 56, 344-350.
- 52 Y. Jia, X. Zhang, Y. Chen, X. Jiang, J. Song, Z. Lin and X. Zhang, Inorg. Chem., 2022, 61, 15368-15376.
- 53 M. Cheng, W. Jin, Z. Yang and S. Pan, Chem. Sci., 2022, 13, 13482-13488.
- 54 SAINT, version 7.60A Bruker Analytical X-ray Instruments, Inc.: Madison, WI, 2008.

- 55 G. M. Sheldrick, Acta Crystallogr., Sect. C: Struct. Chem., 2015, 71, 3-8.
- 56 A. L. Spek, J. Appl. Crystallogr., 2003, 36, 7-13.
- 57 S. J. Clark, M. D. Segall, C. J. Pickard, P. J. Hasnip, M. I. J. Probert, K. Refson and M. C. Payne, Z. Kristallogr., 2005, 220, 567-570.
- 58 J. S. Lin, A. Qteish, M. C. Payne and V. Heine, Phys. Rev. B: Condens. Matter Mater. Phys., 1993, 47, 4174-4180.
- 59 A. M. Rappe, K. M. Rabe, E. Kaxiras and J. D. Joannopoulos, Phys. Rev. B: Condens. Matter Mater. Phys., 1990, 41, 1227-1230.
- 60 J. P. Perdew, K. Burke and M. Ernzerhof, Phys. Rev. Lett., 1996, 77, 3865-3868.
- 61 I. D. Brown and D. Altermatt, Acta Crystallogr., Sect. B: Struct. Sci., 1985, 41, 244-247.
- 62 N. E. Brese and M. O'Keeffe, Acta Crystallogr., Sect. B: Struct. Sci., 1991, 47, 192-197.
- 63 G. Peng, Y. Tang, C. Lin, D. Zhao, M. Luo, T. Yan, Y. Chen and N. Ye, J. Mater. Chem. C, 2018, 6, 6526-6533.
- 64 G. Zou, N. Ye, L. Huang and X. Lin, J. Am. Chem. Soc., 2011, 133, 20001-20007.
- 65 L. Huang, G. Zou, H. Cai, S. Wang, C. Lin and N. Ye, J. Mater. Chem. C, 2015, 3, 5268-5274.
- 66 T. T. Tran, J. He, J. M. Rondinelli and P. S. Halasyamani, J. Am. Chem. Soc., 2015, 137, 10504-10507.
- 67 G. Zou, G. Nam, H. G. Kim, H. Jo, T. S. You and K. M. Ok, RSC Adv., 2015, 5, 84754-84761.
- 68 T. T. Tran, P. S. Halasyamani and J. M. Rondinelli, Inorg. Chem., 2014, 53, 6241-6251.
- 69 G. Zou, C. Lin, H. G. Kim, H. Jo and K. M. Ok, Crystals, 2016, 6, 42.
- 70 A. Adam and V. Cirpus, Z. Anorg. Allg. Chem., 1996, 622, 2023-2030.
- 71 B. Albert, J. Arlt and M. Jansen, Z. Anorg. Allg. Chem., 1992, **607**, 13-18.
- 72 A. V. Yatsenko, S. G. Zhukov, V. A. Dyakov and H. Schenk, Acta Crystallogr., Sect. C: Cryst. Struct. Commun., 1996, C52, 1-3.
- 73 Q. Liu, Z. Li, Y. Wang, X. Su, Z. Yang and S. Pan, Dalton Trans., 2017, 46, 6894-6899.
- 74 C. Bois, G. Papin and M. Philoche-Levisalles, Rev. Chim. Miner., 1984, 21, 152-158.